Applied Ocean Research 129 (2022) 103374

Contents lists available at ScienceDirect

Applied Ocean Research

journal homepage: www.elsevier.com/locate/apor

A probabilistic method to evaluate bow foils for realistic seas and shipping routes

J.A. Bowker *, N.C. Townsend

Faculty of Engineering and Physical Sciences, University of Southampton, UK

ARTICLE INFO

Keywords:
Wave energy
Ship propulsion
Wave augmented propulsion
Bow foils
CO2 emissions
Energy efficiency

ABSTRACT

To improve ship efficiency and reduce CO_2 emissions, the use of renewable based energy saving devices is an emerging field. By harnessing the ambient wave energy, ship bow mounted foils can serve as an energy saving device (ESD), reducing the added resistance in waves and generating an additional thrust. This paper presents a methodology to predict the efficiency of bow foils over various regions, seasons and ship routes. The results show that ship length significantly influences the effectiveness of bow foils with respect to differing regions worldwide. The percentage foil retraction is also shown to be a significant factor in operating bow foils with a large variation depending on ship heading and encountered sea state. The presented method, which could be implemented for the assessment of future bow foil designs, provides a holistic approach to evaluate bow foils for route and ship specific energy savings.

1. Introduction

The advantages of mounting foils at the bow of ships are twofold; to reduce ship heave and pitch motions and improve the propulsive efficiency in a seaway (Jakobsen, 1981; Naito et al., 1986). Both actions result in an overall reduction in ship delivered power (Bowker and Townsend, 2022). Bow foils can therefore act as an energy saving device (ESD) to reduce emissions in the shipping industry.

Full scale sea trials have been conducted by Nikolaev et al. (1995), Terao and Isshiki (1991) and Dybdahl (1988) and bow foils have been operated commercially onboard ferries (Wavefoil, 2019). Scientific research has included both experimental (Bockmann and Steen, 2014; Huang et al., 2016) and numerical studies (Belibassakis and Filippas, 2015; Belibassakis and Politis, 2013; De Silva and Yamaguchi, 2012). More specifically, research has focused on a range of aspects including anti-pitching fins on ships (Abkowitz, 1959; Stefun, 1959; Wu et al., 1996), numerical prediction (Bockmann and Steen, 2016; Isshiki and Murakami, 1984), foil pitch mechanism (Bockmann and Steen, 2014; Naito and Isshiki, 2005), size and location (Feng et al., 2014; Naito and Isshiki, 2005), ship coupling (Bowker et al., 2021; Filippas, 2015; Feng et al., 2014), resistance and propulsion (Belibassakis et al., 2021; Feng et al., 2014), oblique waves (Feng et al., 2014) and free surface effects (Filippas et al., 2020).

In order to assess the benefits of fitting or retrofitting bow foils, stakeholders require an understanding of bow foil performance in realistic seas. Realistic seas refers to the ambient wave energy encountered by a ship for the intended or current shipping route. Previous methods by Naito and Isshiki (2005), Feng et al. (2014) and Bockmann et al. (2018) have undertaken numerical simulations to calculate the effect of bow foils on ship propulsion and motions in realistic waves. In all cases, strip theory was employed to resolve the ship motions in the frequency domain, which could then be transferred to evaluate the forces acting on the bow foil. To resolve the coupled effect, Naito and Isshiki (2005) accounted for the effect of the foil on the ship motions by including the foil forces in the ship equation of motion. The foil lift and thrust forces in a wavy flow were determined using Theodorsen's unsteady foil theory. Combining this with the added resistance in waves, Naito and Isshiki (2005) was able to predict the speed loss in irregular waves for with and without a bow foil. To resolve the effect of bow foils on the ship's engine load and speed, Feng et al. (2014) expanded the coupled solution by combining the ship-foil response with propulsive coefficients, then implemented this method to evaluate the effect of bow foils on a ship's engine load for a specific route, accounting for wave statistics. This method was advanced by Bockmann et al. (2018) to include the effect of dynamic stall on the foil lift forces for large angles of attack, which was achieved using a hybrid time domain solution. Strip theory was used to resolve the ship-foil coupling and a dynamic stall theory was used to evaluate the foil forces at each time step. To assess the effect of the bow foil, Bockmann et al. (2018) predicted the ship's engine load by evaluating the change in total resistance due to foil thrust and reduced added resistance in waves. Alternative methods include the direct measurement approach developed by Bowker and

* Corresponding author.
E-mail addresses: J.Bowker@soton.ac.uk (J.A. Bowker), nick@soton.ac.uk (N.C. Townsend).

https://doi.org/10.1016/j.apor.2022.103374
Received 14 July 2022; Received in revised form 8 September 2022; Accepted 6 October 2022
Available online 23 October 2022

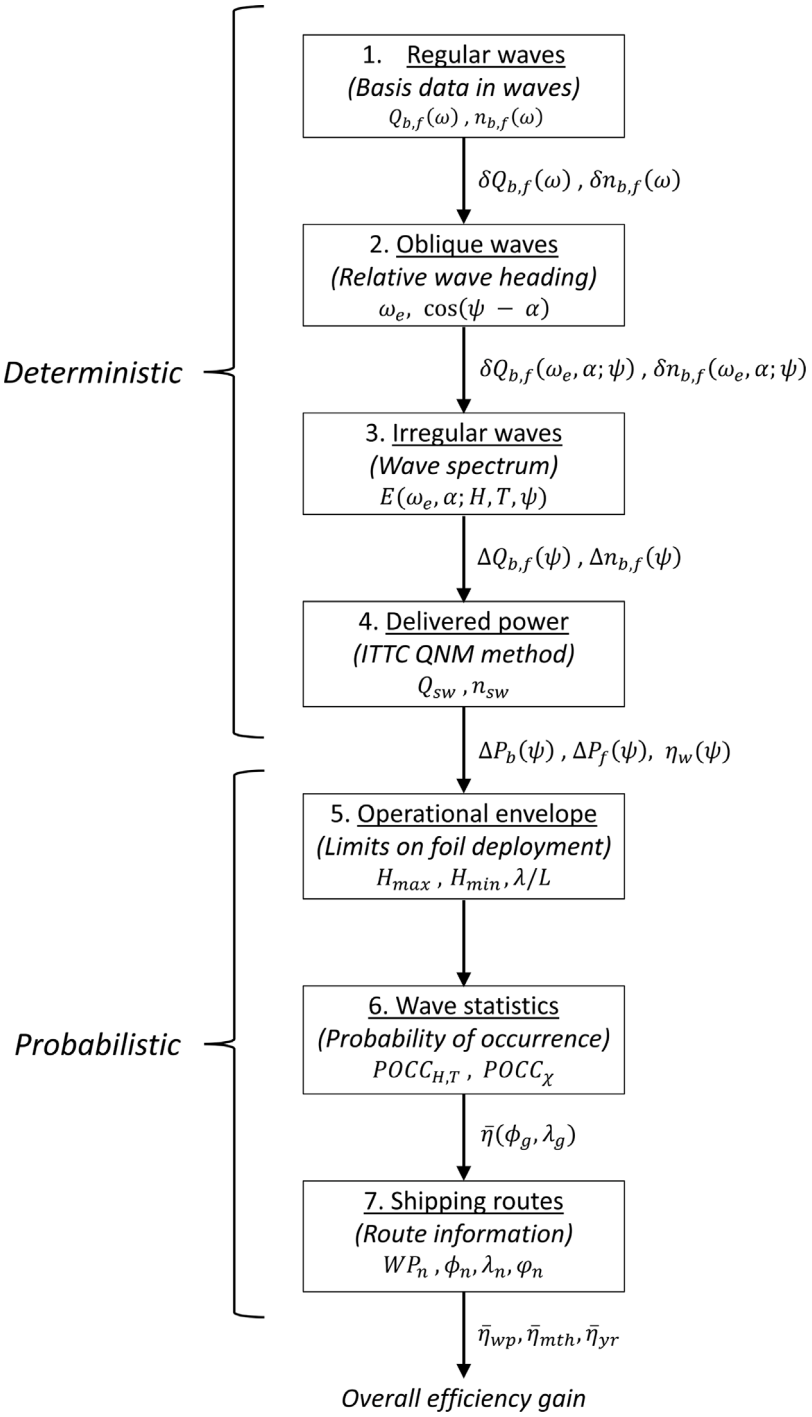

Fig. 1. Flowchart illustrating the numerical process.

Townsend (2022), which accounts for the ship-foil coupling, the change in added resistance in waves and foil thrust as a holistic response on the ship's engine load over a range of regular wave frequencies.

A numerical method was presented by Feng et al. (2014) to assess the performance of bow foils for a ship route in the North Pacific including wave statistics. This method combines the spectral ship-foil response with the probability of occurrence for a particular sea state, assuming head seas. The heading contribution was weighted equally across all directions, resulting in a 1/9 probability of foil effectiveness in head seas (160–180 deg). In order to evaluate the effect of bow foils on the ship's CO_2 emissions in realistic seas, Feng et al. (2014) calculated the ship's Energy Efficiency Design Index (EEDI) for with and without foils. Contrastingly, Bockmann et al. (2018) implemented a Monte Carlo approach to investigate the effect of bow foils in realistic seas. Using the hybrid time domain numerical model, Bockmann et al. (2018) completed 1000 simulations per route for two ships, one with a bow foil and the other without. During the simulations, the foils were retracted if the propulsive efficiency became less than that of the ship without a foil. The results were then compiled to produce histogram probability distributions of the fuel savings for each route. The simulations were also performed for a range of ship speeds, resulting in a mean fuel saving per speed for each route.

Through experiments, simulations and full scale trials, the use of bow foils has been shown to significantly reduce a ship's delivered

power in waves. Although this amounts to a considerable volume of research and development, the number of studies that have assessed bow foils in realistic seas (historical or hindcast wave data) are limited to several articles with vastly different predictions for fuel savings (1.6% Feng et al., 2014 vs. 22 % Bockmann et al., 2018). However, these predictions cannot be considered equivalent due to the considerable difference in methodology, ship length (214 m Feng et al., 2014 vs. 100 m Bockmann et al., 2018), location (North Pacific Ocean Feng et al., 2014 vs. North Eastern Atlantic Ocean Bockmann et al., 2018) and foil size (1% of waterplane area Feng et al., 2014 vs. 2.6% Bockmann et al., 2018). Both (probabilistic) methods provide a useful approach for evaluating bow foil performance in realistic seas. These methods are based on numerical predictions, which have shown promising comparisons against experimental results. However, given the considerable differences noted between the numerical predictions of Feng et al. (2014) and Bockmann et al. (2018), a more direct method based on experimental data is absent from the research domain.

1.1. Paper contribution and outline

Using spectral analysis and ocean wave statistics, this paper presents a methodology to predict the effect of bow foils on a ship's powering demand for particular shipping routes in representative waves (irregular and oblique), which forms an extension on the previous research in regular waves (Bowker and Townsend, 2022). A spectral analysis method (using the measured data from physical experiments Bowker and Townsend, 2022) is combined with ocean wave statistics to estimate the mean efficiency gain from bow foils (calculated as the difference in delivered power between a ship with and without bow foils) for a range of ship sizes (75 m to 150 m in length), over various shipping routes, in representative oblique, short crested waves.

The method, which predicts the change in delivered power in irregular short-crested waves, uses wave data to provide a global assessment and predict the performance of bow foils for a range of shipping routes and ship sizes. More specifically, the statistical analysis includes the relative wave heading with respect to the ship's heading (for example, east vs. westbound in the North Atlantic) and percentage foil retraction, which is an extension on the method presented by Feng et al. (2014). Although the results in this paper are limited to the specific particulars of the basis experimental data, the methodology outlined in the following sections could be applied to prospective bow foil designs in the support of EEDI index certification (ITTC, 2021a).

The paper is structured as follows: Section 2 outlines the methodology, basis dataset, theory, wave statistics and shipping routes. The results are presented in Section 3 including a global assessment of the overall bow foil efficiency gain projections for ship size and routes. A discussion of the results is given in Section 4.

2. Methodology

The methodology follows a series of numerical processes, which combines the deterministic evaluation of bow foils in waves with the probabilistic analysis of waves statistics and shipping routes, as illustrated in Fig. 1 and summarised in the following text:

1. ***Regular waves:*** Compile experimental dataset in regular waves across a range of wave frequencies which encompasses the bow foil effectiveness (i.e. positive efficiency gain)
2. ***Oblique waves:*** Extend the analysis in the previous step to account for the change in bow foil performance in additional relative wave headings (e.g. bow-quartering waves)
3. ***Irregular (short-crested) waves:*** Using spectral analysis, predict the change in propeller torque and revolutions for with and without the bow foil in irregular, short-crested waves
4. ***Delivered power:*** Following the International Towing Tank Committee (ITTC) torque-RPM (QNM) method (ITTC, 2021b), calculate the change in delivered power in waves for with and without the bow foil and, therefore, estimate the resultant efficiency gain and reduction in fuel consumption and CO_2 emissions
5. ***Operational envelope:*** Place limits on the sea states for which bow foils are deployed (i.e. minimum and maximum wave height and wave period)
6. ***Wave statistics:*** Compile wave scattergrams from global wave statistics (e.g. WaveWatch III NOAA, NCEP, 2021) for all locations and combine the previous analysis with the probability of occurrence to predict the performance of bow foils around the globe
7. ***Shipping routes:*** Define shipping routes using waypoints and ship headings, then apply wave statistics for each waypoint to assess the performance of bow foils on outbound and return voyages

Table 1
Ship and bow foil dimensions for a range of length scales.

Ship/Foil particular	Model scale	Case 1	Case 2	Case 3	Case 4
Length [m]	2	75	100	125	150
Displacement [kg]	51.50	2.78×10^6	6.60×10^6	1.29×10^7	2.23×10^7
Beam [m]	0.173	12.375	16.500	20.625	24.750
Draught [m]	0.12	4.50	6.00	7.50	9.00
Vertical CoG [m] (from keel)	0.14	5.25	7.00	8.75	10.50
Longitudinal CoG [m] (forward of amidships)	0.005	0.188	0.250	0.313	0.375
Foil span [m]	0.42	15.75	21.00	26.25	31.50
Foil chord [m]	0.06	2.25	3.00	3.75	4.50
Speed (kts)	1.56	9.52	11.00	12.30	13.47
Delivered power (W)[a]	2.36	354×10^3	903×10^3	1888×10^3	3427×10^3

[a]Estimated for calm water using the Holtrop formulations for total resistance and a quasi propulsive efficiency of 0.59.

2.1. Regular waves

The research presented in this paper utilises the experimental results from model scale tests in regular waves published by Bowker and Townsend (2022). The experiments were conducted using a free running model, shown in Fig. 2, with a bow foil mounted at 10% model length beyond the forward perpendicular and plan area of 4.6% of the ship's waterplane area.

The model dimensions, derived from the basis data of realistic bulk carriers, are presented in Table 1 along with the full scale equivalent values for a range of length scales (L = 75 m to 150 m). The scaling method assumes Froude scaling laws and kinematic similarity such that the foil pitch and angle of attack is equivalent at each length scale for a proportional wave amplitude and frequency. Further information and non-dimensional parameters are published in the preceding article by Bowker and Townsend (2022).

A constant speed was maintained in waves by controlling the propeller revolutions (rpm) using a proportional–integral feedback controller. To ensure that the demanded rpm was in response to the added resistance due to waves, the model's feedback speed was filtered using a low-pass filter to eliminate the effect of individual waves on the controller. For a range of regular wave frequencies (ω) and for with and without the bow foil, the propeller torque ($Q_{b,f}(\omega)$) and revolutions per second ($n_{b,f}(\omega)$) were recorded using a torquemeter and shaft encoder, respectively. The subscript b refers to the ship with a bare hull, i.e. without a foil, and f refers to the ship with a bow foil installed.

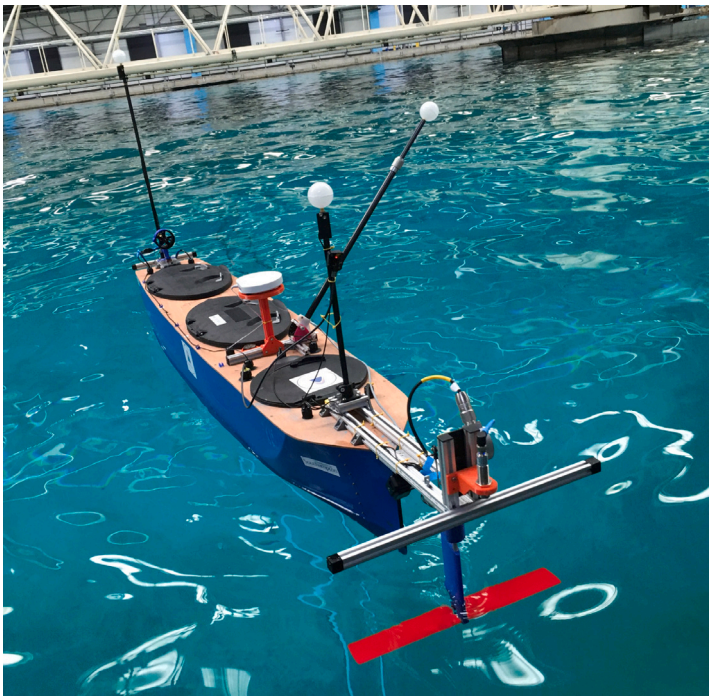

Fig. 2. Image of the free running model developed by Bowker and Townsend (2022).

2.2. Oblique waves

For the purposes of this study, the propulsive measurements in waves have been adjusted to be a function of wave direction by applying a cos-squared relationship (as observed by Bowker and Townsend, 2022 during turning circle manoeuvres in waves). This assumes that the bow foil effectiveness is a function of the cos-squared deterioration from head seas through to beam seas, and zero effectiveness in beam through to following seas:

$$\begin{aligned} Head\ seas,\ \ cos(\psi-\alpha)>0: \quad & \delta Q_{b,f}(\omega_e,\alpha;\psi)=\delta Q_{b,f}(\omega_e) \\ & \times cos^2(\psi-\alpha) \\ & \delta n_{b,f}(\omega_e,\alpha;\psi)=\delta n_{b,f}(\omega_e) \\ & \times cos^2(\psi-\alpha) \\ Following\ seas,\ \ cos(\psi-\alpha)<0: \quad & \delta Q_{b,f}(\omega_e,\alpha;\psi)=0 \\ & \delta n_{b,f}(\omega_e,\alpha;\psi)=0 \end{aligned} \tag{1}$$

Importantly, the wave encountered frequency is also adjusted for each relative wave direction:

$$\omega_e=\omega+\frac{\omega^2 U}{g}cos(\psi-\alpha) \tag{2}$$

2.3. Irregular (short-crested) waves

To predict the response in irregular waves, the current method utilises an extension of the International Towing Tank Committee (ITTC) torque-rpm (QNM) formulations (ITTC, 2021b). The ITTC QNM method utilises experimental measurements in regular waves (propeller torque and revolutions) to predict the spectral response ($\delta Q_{b,f}, \delta n_{b,f}$) in irregular waves, as explained in ITTC (2021b). The change in torque ($\delta Q(\omega)$) and propeller revolutions ($\delta n(\omega)$) were evaluated at each wave frequency relative to the calm water results without the bow foil (Q_{sw}, n_{sw}), then integrated over the range of encountered wave frequencies (ω_e) and the relative headings of short crested waves (α), for each relative wave direction (ψ):

$$\Delta Q_{b,f}(\psi)=2\int_{-\pi/2}^{\pi/2}\int_0^{\infty}\frac{\delta Q_{b,f}(\omega_e,\alpha;\psi)}{\zeta^2}E(\omega_e,\alpha;H,T,\psi)d\omega_e d\alpha \tag{3}$$

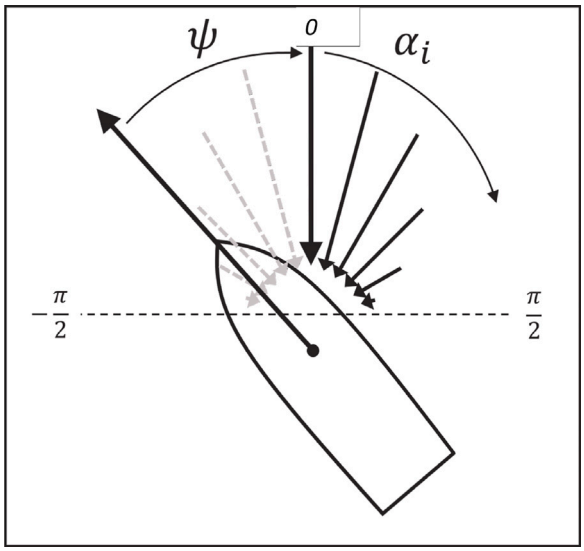

Fig. 3. Definition of relative wave heading (ψ) and direction (α_i).

$$\Delta n_{b,f}(\psi)=2\int_{-\pi/2}^{\pi/2}\int_0^{\infty}\frac{\delta n_{b,f}(\omega_e,\alpha;\psi)}{\zeta^2}E(\omega_e,\alpha;H,T,\psi)d\omega_e d\alpha \tag{4}$$

where ζ is the regular wave amplitude and E is the directional wave spectrum, which is a function of the encountered frequency spectrum ($S(\omega_e)$) and directional spreading function ($D(\alpha)$):

$$E=S(\omega_e)D(\alpha) \tag{5}$$

For a given ship route, the ship will encounter a predominant wave direction relative to the ship's heading, referred to as the relative wave direction, illustrated in Fig. 3. In addition to the predominant wave direction, the ship also encounters waves from a spread of other wave directions which forms short-crested waves, also illustrated in Fig. 3.

Ocean measurements show that the spreading of waves from different directions can vary depending on several factors but a typical approximation for the open ocean is a cosine-squared spreading function (Cummins and Bales, 1980). This function spreads the total wave spectra about the predominant wave direction at a deteriorating rate approaching zero energy at a relative angle of 90 degrees:

$$D(\alpha) = \frac{2}{\pi} cos^2 \alpha \tag{6}$$

2.4. Delivered power

The change in torque and propeller revolutions are combined to calculate the overall change in delivered power in an irregular wave ($\Delta P_{b,f}$), which was then used to estimate the change in propulsive efficiency in waves due to the bow foil (η_w):

$$\Delta P_{b,f}(\psi) = 2\pi[(Q_{sw} + \Delta Q_{b,f}(\psi))(n_{sw} + \Delta n_{b,f}(\psi)) - Q_{sw} n_{sw}] \tag{7}$$

$$\eta_w(\psi) = \frac{\Delta P_b(\psi) - \Delta P_f(\psi)}{P_{sw} + \Delta P_b(\psi)} \tag{8}$$

The efficiency gain is given as the difference between the delivered power required in a sea state for with and without a bow foil. Alternatively, by applying fuel consumption rates (SFC_{ME}) and carbon emission factor (CF), it is possible to convert the change in delivered power into an estimate for fuel consumption ($\Delta Fuel$) and emissions savings (ΔCO_2):

$$\Delta Fuel = \left(\Delta P_f(\psi) - \Delta P_b(\psi)\right) \times SFC_{ME} \times h \tag{9}$$

where h is voyage time in hours. The emissions saving can then be estimated as follows:

$$\Delta CO_2 = \Delta Fuel \times CF \tag{10}$$

Since the analysis presented in this article is applied to a generic hull design, the reference values from the International Maritime Organization (IMO) Marine Environment Protection Committee (MPEC) guidelines (IMO, 2013) have been implemented for specific fuel consumption (190 g/kWh) and emissions factor (3.1144 gCO_2/g).

2.5. Operational envelope

In this study, the foils were assumed to be retracted beyond an operational envelope which is defined by practical limits. The following rules were set as practical limits:

- ***Maximum wave steepness:*** For structural integrity, the bow foil was assumed to be retracted in sea states with a steepness greater than 1/20 for the shortest wavelength to ship length ratio (0.8):

$$H_{max} = \frac{1}{20} \times 0.8 \times \lambda / L \tag{11}$$

- ***Minimum wave height:*** Sea states with a significant wave height less than 1 m were assumed to be equivalent to calm water conditions, for which the foil is retracted to eliminate the additional drag.

- ***Minimum and maximum wave period:*** The bow foil was retracted for sea states that result in a negative efficiency gain due to a mean wave period beyond the range of bow foil effectiveness, as shown in the experimental results in Bowker and Townsend (2022):

$$\lambda / L \ll 0.8 \qquad \lambda / L \gg 1.6 \tag{12}$$

- ***Relative wave heading:*** The turning circle observations made by Bowker and Townsend (2022) show that the bow foil is ineffective in following seas and it was therefore assumed that the foil would be retracted in relative wave headings that range from beam seas through to following seas.

Through application of these limits, operational envelopes have been generated for varying ship sizes from 75 m to 150 m, shown in Fig. 4. Using wave statistics and ship route information, discussed in the following sections, this method is able to predict the percentage time that the foil is retracted due to sea states being beyond the operational envelope of the bow foil or due to following seas.

2.6. Wave statistics

The WaveWatch III 31 year hindcast dataset is available online for the global oceans (NOAA, NCEP, 2021), the North Sea and the Mediterranean Sea, with a geographic coordinate grid resolution of 1/2°, 3/12° and 1/6°, respectively. For the years from 1979 to 2009, data on the significant wave height (H), mean wave period (T) and wave direction (χ) have been downloaded in the form of GRIdded BInary (GRIB) files. The open source program called NCTOOLBOX (Schlining et al., 2009) was utilised to read the data stored in each GRIB file.

The wave data was compiled using MATLAB, which loops through each year, month and wave parameter to generate a histogram for every geographic grid coordinate in each region. Following the guidance provided by Perrault (2021), the method uses a long duration of observations (31yrs) and the finest resolution available for latitude and longitude and the shortest time interval between measurements (3 h). In order to limit the required computational capacity, the bin widths for the significant wave height, mean wave period and wave direction were set to 1 m, 2 s and 15 deg, respectively. A sensitivity study on bin width has been completed at finer resolutions (0.5 m, 1 s and 5 deg) and is included in the uncertainty analysis. Fig. 5 presents an example scattergram for the wave height and period and an example polar histogram for the wave direction.

From this analysis, the probability of occurrence for each sea state ($POCC_{H,T}$) and wave direction ($POCC_\chi$) for a particular time of the year and location is calculated using the counts (m) for each histogram bin:

$$POCC_{H,T} = \frac{m_{H,T}}{\sum m_{H,T}} \tag{13}$$

$$POCC_\chi = \frac{m_\chi}{\sum m_\chi} \tag{14}$$

With the introduction of ship routing, the ship's heading (φ) can be used to generate the probabilities of occurrence for each relative wave heading ($POCC_\psi$):

$$POCC_\psi(j) = POCC_\chi(j = \chi - \varphi) \quad where\ j = 0°, 15°, 30°, \ldots, 330° \tag{15}$$

The results from the spectral analysis for the bow foil efficiency gain in irregular short crested waves were applied for each relative wave heading and sea state, then combined with the probability of occurrence for each wave direction to calculate the mean efficiency gain for each sea state at every longitude and latitude location (ϕ_g, λ_g):

$$\eta_\psi(H, T, \phi_g, \lambda_g) = \sum_{i=\pi/12}^{2\pi} \eta_w(H, T, \psi_i) \times POCC_{\psi_i}(\phi_g, \lambda_g) \tag{16}$$

For assessing the overall outlook of a particular ocean or sea, the ship heading cannot be included in the analysis and, therefore, the probability of occurrence for relative wave heading was set to an equal probability of 1/24 (15°/360°). The total efficiency gain for a particular location was calculated by multiplying the efficiency gains for each sea state within the operational envelope:

$$\overline{\eta}_{total}(\phi_g, \lambda_g) = \sum_{i=1}^{10} \eta_\psi(H_i, T_i, \phi_g, \lambda_g) \times POCC_{H_i,T_i}(\phi_g, \lambda_g) \tag{17}$$

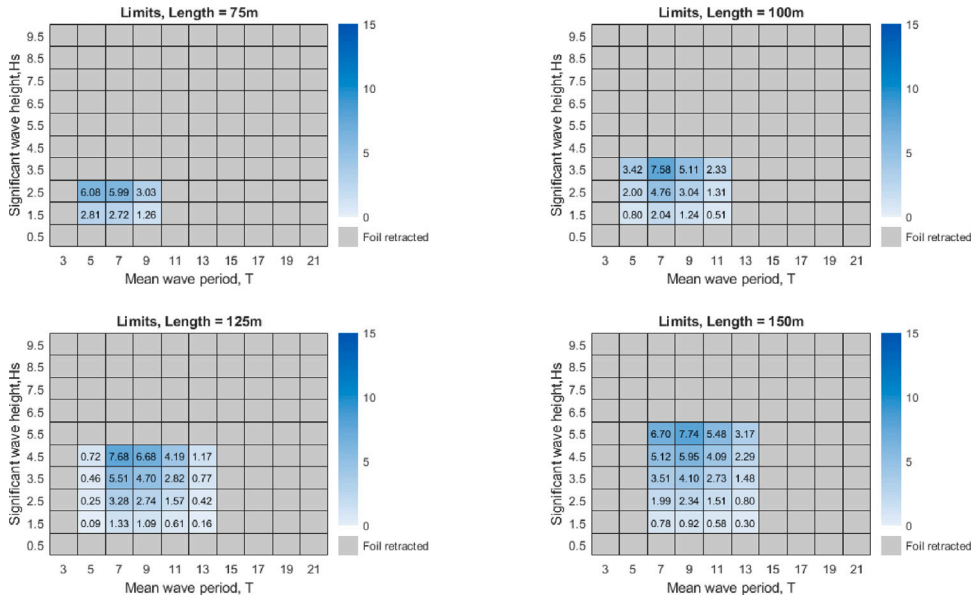

Fig. 4. Example of the operational envelopes for ship lengths 75 m to 150 m including the bow foil efficiency gains for each sea state (assuming an equal probability of occurrence for relative wave direction).

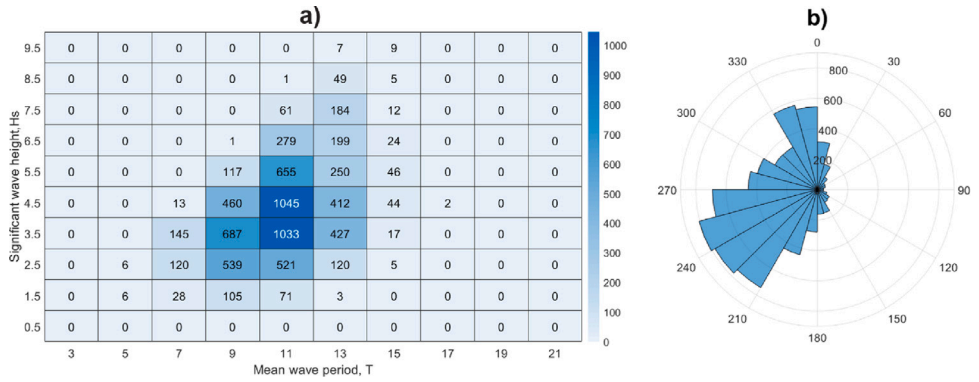

Fig. 5. Example histogram data for (a) the significant wave height and period and (b) the wave direction for a location in the North Atlantic (45°N, 45°W) during the month of January for 31 years between 1979 and 2009.

Table 2
Shipping route information and total distance.

Route	Start		End		No.	Nautical
	Latitude	Longitude	Latitude	Longitude	waypoints	miles
North Atlantic	28°0′0″N	77°0′0″W	49°0′0″N	8°30′0″W	60	3330
North Pacific	34°0′0″N	143°0′0″E	38°30′0″N	125°30′0″W	60	4240
North Sea	53°30′0″N	0°30′0″E	54°0′0″N	8°0′0″E	30	268
Mediterranean Sea	36°0′0″N	4°0′0″E	32°30′0″N	31°30′0″E	60	1763

2.7. Shipping routes

The final section of the methodology involves the definition and inclusion of shipping routes. Exemplar shipping routes with high traffic (Wu et al., 2017) have been selected as case studies to cover the following regions; the North Pacific Ocean, the North Atlantic Ocean, the North Sea and the Mediterranean Sea, as summarised in Table 2 and plotted in Fig. 6.

Each route follows an orthodromic course for the most direct route and is divided into a series of waypoints, each with a longitude, latitude and heading. The number of waypoints was set to ensure that the resolution was similar to the grid coordinates in the WaveWatch III dataset so that each waypoint utilised the nearest wave data.

For each waypoint (WP_n), the overall efficiency gain was calculated for each month of the year and for both the outbound and return journey with the only difference being the ship heading:

$$\overline{\eta}_{wp}(WP_n, Month) = \overline{\eta}_{total}(\phi_n, \lambda_n, \varphi_n) \tag{18}$$

The resultant overall monthly and yearly efficiency gain for each route was calculated as the mean of all the waypoints and months, respectively:

$$\overline{\eta}_{mth}(Route, Month) = \frac{\sum_{n=1}^{N} \overline{\eta}_{wp}(WP_n, Month)}{N} \tag{19}$$

$$\overline{\eta}_{yr}(Route) = \frac{\sum_{1}^{12} \overline{\eta}_{mth}(Route, Month)}{12} \tag{20}$$

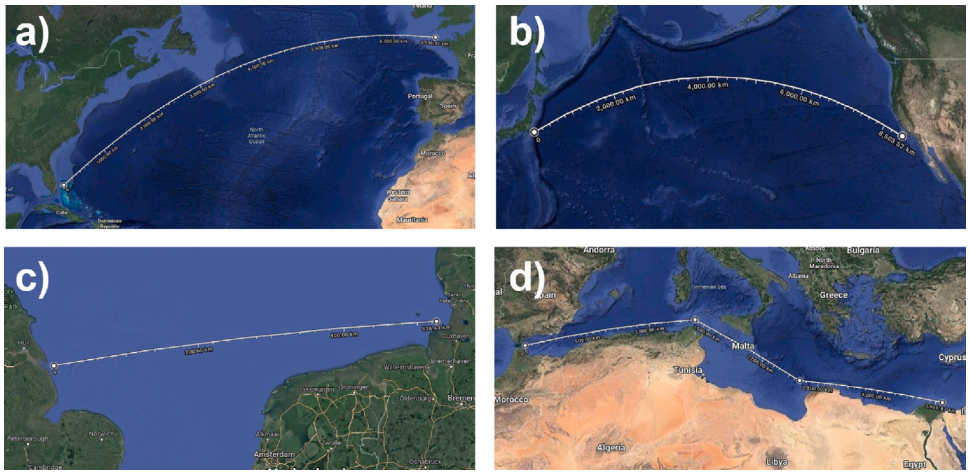

Fig. 6. Case study shipping routes: (a) North Atlantic (Gulf of Mexico to the English Channel); (b) North Pacific (Tokyo to San Francisco); (c) North Sea (Hamburg to Hull); (d) Mediterranean Sea (Gibraltar Strait to the Suez Canal).

With the introduction of ship routing and heading, the percentage foil retraction (FR) was calculated using both the probability of occurrence for relative wave direction ($POCC_{\psi}$) and sea state ($POCC_{Hs,T}$):

$$\begin{aligned} \%\,FR = 100\times \Big(& \sum POCC_{\psi}(Following\ seas) \\ & + \Big[1 - \sum POCC_{\psi}(Following\ seas)\Big] \\ & \times \sum POCC_{Hs,T}(Hs,T\ beyond\ OE) \Big) \end{aligned} \tag{21}$$

3. Results

3.1. Uncertainty

To assess uncertainty, the results include three main sources; experimental uncertainty, statistical uncertainty and numerical uncertainty. The experimental uncertainty (u_E) is associated with the accuracy and repeatability of measurements at model scale. The ITTC published a procedure (ITTC, 2014) for calculating experimental uncertainty based on the ISO-GUM guidelines (International Organisation for Standardisation, Guide to the Expression of Uncertainty in Measurements). The ITTC procedures and guidelines define two types of experimental uncertainty; Type A and Type B. Type A is derived from the uncertainty of repeat measurements and Type B includes elemental uncertainties pertinent to the sensors, calibration, data acquisition, processing and analysis.

The statistical uncertainty (u_W) is due to the variability of ambient wave energy for a particular shipping route. The numerical uncertainty (u_R) is the numerical resolution of the statistical analysis, which includes the wave data temporal and spatial resolution, the basis data resolution (i.e. wave frequency intervals) and the bin width for the statistical analysis. The total uncertainty (u) was evaluated as the sum of uncertainties:

$$u = \sqrt{u_E^2 + u_W^2 + u_R^2} \tag{22}$$

In this case, the experimental uncertainty was estimated following the method outlined by Bowker and Townsend (2022) which implements a Type A uncertainty using a Student's t value ($t = 2.92$) and a Type B sensor uncertainty (4.32%). The statistical uncertainty due to yearly variation (u_Y) has been estimated for each shipping route by calculating the overall efficiency gain for each year of wave statistics, then evaluating the standard uncertainty with a 95% confidence interval from 31 years of wave data (1979–2009):

$$u_Y = 1.96 \times \frac{1}{N} \sum_{yr=1}^{N} (\eta_{yr} - \bar{\eta})^2 \tag{23}$$

The same method has been used to estimate the standard uncertainty for monthly or seasonal variation (u_M) throughout the year using the 31 year mean annual efficiency gain for each month and route:

$$u_M = 1.96 \times \frac{1}{N} \sum_{mth=1}^{N} (\eta_{mth} - \bar{\eta})^2 \tag{24}$$

The total standard uncertainty due to the statistical variation of waves is then estimated as the sum of both the annual and seasonal variation:

$$u_W = \sqrt{u_Y^2 + u_M^2} \tag{25}$$

The numerical uncertainty (u_R) has been evaluated for the scattergram bin width, which was estimated for each route by comparing high (0.5 m, 1 s and 5 deg) and low (1 m, 2 s and 15 deg) resolutions for 31 years of wave data, during the month of January (selected to be indicative of the remaining dataset):

$$u_R = \frac{|\eta_{high} - \eta_{low}|}{2} \tag{26}$$

An overview of the contributions from each type of uncertainty is shown in Fig. 7, which highlights that the numerical uncertainty is almost negligible (≈1%) compared to the experimental and statistical uncertainty. The statistical uncertainty is shown to have the largest contribution which is understandable given the variability of ambient wave energy. The total uncertainty has been included in the results as upper and lower bounds relative to the mean annual bow efficiency gain, assuming a normal distribution.

3.2. Global assessment

Fig. 8 presents the projected efficiency gains due to bow foils for a range of ship sizes from 75 m to 150 m length. Since the operational envelope is governed by the wavelength to ship length ratio, the ideal sea state is dependent on ship length.

The results highlight the dominance of ship length scale on the performance of bow foils, particularly with respect to operational regions across the globe. For example, it is predicted that bow foils would be suitable on 'Handysize' and 'Handymax' bulk carriers (L = 130–200 m) for voyages across the North Atlantic and Pacific Oceans and in the Southern Ocean. Whereas, 'Small' bulk carrier (L = 75–125 m) could operate with bow foils in regions with a short fetch, such as the North Sea.

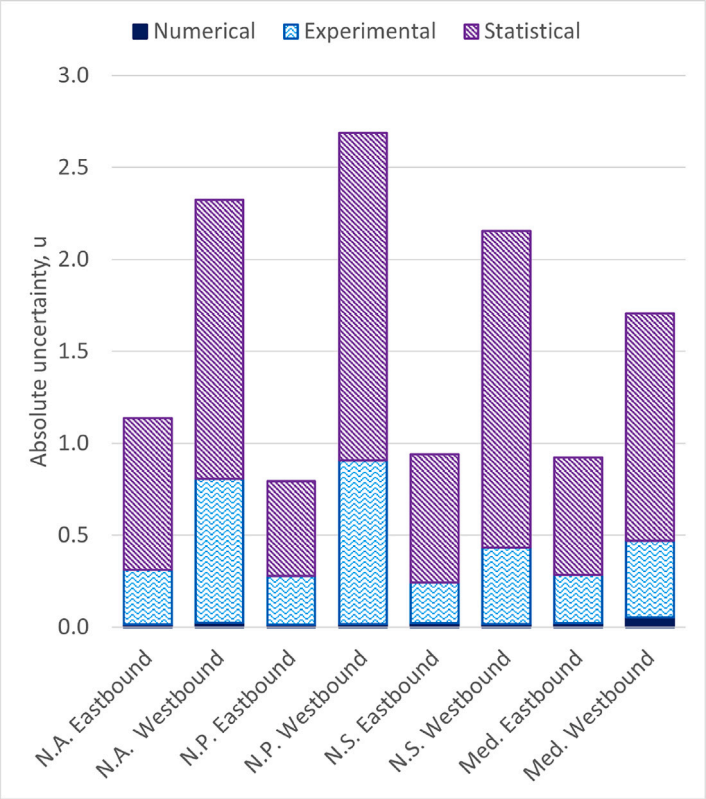

Fig. 7. Contributions to overall uncertainty for each route (North Atlantic (N.A.), North Pacific (N.P.), North Sea (N.S.) and Mediterranean (Med)).

Table 3
Summary of annual mean bow foil efficiency gains and fuel reductions for each route, including estimated upper and lower bounds.

Route	Ship	Efficiency gain (%)			Reduction[b] (t)		Retraction
(Direction)	case[a]	Lower	Mean	Upper	Fuel[c]	Emissions[d]	(%)
North Atlantic (Eastbound)	4	0.31	1.19	2.06	−6.25	−19.47	68.31
North Atlantic (Westbound)	4	1.38	3.11	4.79	−17.63	−54.91	40.53
North Pacific (Eastbound)	4	0.47	1.06	1.63	−5.72	−17.81	74.30
North Pacific (Westbound)	4	1.41	3.43	5.40	−19.71	−61.38	36.21
North Sea (Eastbound)	2	0.21	0.94	1.67	−0.12	−0.39	74.90
North Sea (Westbound)	2	0.02	1.80	3.56	−0.24	−0.75	59.51
Mediterranean (Eastbound)	1	0.41	1.11	1.79	−0.42	−1.32	83.10
Mediterranean (Westbound)	1	0.43	1.75	3.05	−0.67	−2.10	74.63

[a]In reference to Table 1.
[b]Estimated in tonnes per voyage as a seasonal average.
[c]Specific fuel consumption = 190 g/kWh (from the reference value in MPEC.231(65)) (IMO, 2013).
[d]Emissions factor = 3.1144 CO2g/g fuel (from the reference value in MPEC.231(65)) (IMO, 2013).

3.3. Shipping routes

The following section presents the bow foil efficiency gain projections for the shipping routes outlined in Section 2.7. Table 3 summarises the annual mean bow foil efficiency gain for each route with upper and lower bounds from the uncertainty analysis. Table 3 also contains the estimated mean reduction in fuel and CO_2 emissions due to the deployment of the bow foil, and presents the mean percentage foil retraction for each voyage.

Figs. 9, 10, 11 and 12 present the seasonal and enroute variation in efficiency gain and percentage foil retraction. The results show a significant variation along the route and throughout the year, depending on the seasonal weather patterns with up to 5% reduction in delivered power.

4. Discussion

4.1. Global outlook

The global assessment shows that the ship length is the governing parameter with regard to bow foil effectiveness, which highlights the importance of matching the bow foil application to the ship type and region of operation. In this generalised assessment the ship is assumed to encounter waves from all headings with equal probability. However, as shown in the ship route analysis, certain ship headings are preferable due to prevailing wave systems and the results are therefore likely to underestimate the efficiency gain for certain shipping routes.

For optimal application, the results show that the highest efficiency gains could be attained in the Southern Ocean, which completes a full circuit of the globe with no landmass to inhibit the development of

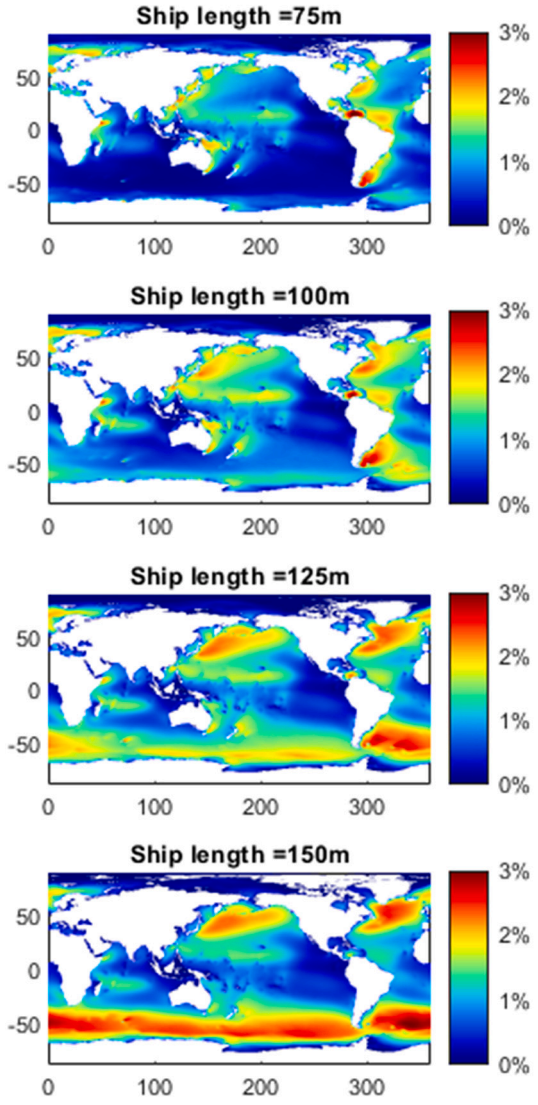

Fig. 8. Global outlook for bow foil efficiency gain for increasing ship size (75 to 150 m).

large sea states. However, the shipping traffic in the southern ocean is minimal and operating in this region is impractical. Both the North Pacific and North Atlantic show promising results for 150 m ships and reasonable efficiency gains could be achieved for small ships in short sea zones such as the North Sea, the Sea of Japan and the Caribbean Sea.

4.2. Variation

Fig. 13 presents a summary of the statistical variation of the averaged bow foil efficiency results. Significant variation is observed with respect to the time of the year (i.e. seasonal), the position along the route (i.e. enroute) and the destination (i.e. east vs. westbound).

The seasonal variation generally results in higher efficiency gains during the winter months (October to March) and lower efficiency gains during the summer months (April–September), which is associated with the prevailing global wave patterns in the Northern hemisphere. The enroute variation provides an additional insight into the effect of local wave patterns along the route, which is similar in magnitude to the seasonal variations. The results show a clear mirroring of the efficiency gain relative to the percentage foil retraction, which is shown to increase as the ship approaches the destination port. This could be due to local wave patterns, such as the ship predominantly sailing in following seas (i.e. waves propagating towards the land) or that the fetch is too short for an offshore wind to cause a fully developed sea. Local weather factors are, therefore, shown to significantly affect the bow foil effectiveness, which is particularly noticeable for the Mediterranean Sea.

Furthermore, there is a consistent increase in the overall efficiency gain when heading on westbound routes compared to the eastbound routes, highlighted in Fig. 13. This is evident in the percentage foil retraction due to following seas, which is consistently over 50% for an eastbound route and consistently less than 50% for a westbound route. For short sea regions, such as the Mediterranean Sea, the effect of ship heading is reduced in comparison to the open ocean due to a more evenly distributed wave direction.

There is also a significant variation in the results with respect to the scale of the ship, which shows that higher overall efficiency gains were predicted for the largest ship scale (Case 4) in comparison to the smaller ship scales (Cases 1 & 2). This is partially associated with the wave environment in the open ocean (i.e. North Atlantic and North Pacific) in comparison to the short sea routes (i.e. North Sea and Mediterranean). However, the results also show that the percentage foil retraction due to the occurrence of sea conditions beyond the operational envelope (Beyond OE) is significantly higher for smaller ships (~28%), in comparison to larger ships (~7.5%). This contraction of the operational envelope for smaller ship scales is a mathematical function of scale which further highlights the importance of deploying bow foils on ships that are most likely to operate in waves with an encountered wavelength close to the length of the ship.

4.3. Probability of exceedance

Wave statistics have been implemented to determine the average likely efficiency gain for a given route with consideration for foil retraction, which represents zero efficiency gain and therefore acts to reduce the overall average efficiency gain prediction. This does not, however, give a representative measure of the bow foil efficiency gains when the foil is deployed. To achieve this, the bow foil efficiency gain was predicted for every sea state observed at each waypoint for all routes from the entire 31 year WaveWatch III dataset (within the bounds of the operational envelope). At intervals of half percent, the resultant efficiency gain dataset was binned to generate a histogram record which was then used to calculate the probability of exceeding a particular efficiency gain whilst the bow foil is deployed. These results are presented in Figs. 9(c), 10(c), 11(c) and 12(c) for the case study routes.

The probability of exceedance provides a useful indication on the bow foil effectiveness whilst deployed. For instance, the likely bow foil efficiency gain for the North Atlantic westbound route is predicted to be greater than 5% for 30%–50% of foil deployments.

4.4. Limitations

The presented methodology utilises realistic sea state and shipping route information to derive global and route specific predictions on bow foil efficiency gains and percentage foil retraction. Different configurations, foil size, flapping characteristics and hull shapes would yield variations in the overall predictions. Since the geometrical parameters in this example are fixed in relation to the basis model scale data, it was not possible to investigate the effect of different design parameters

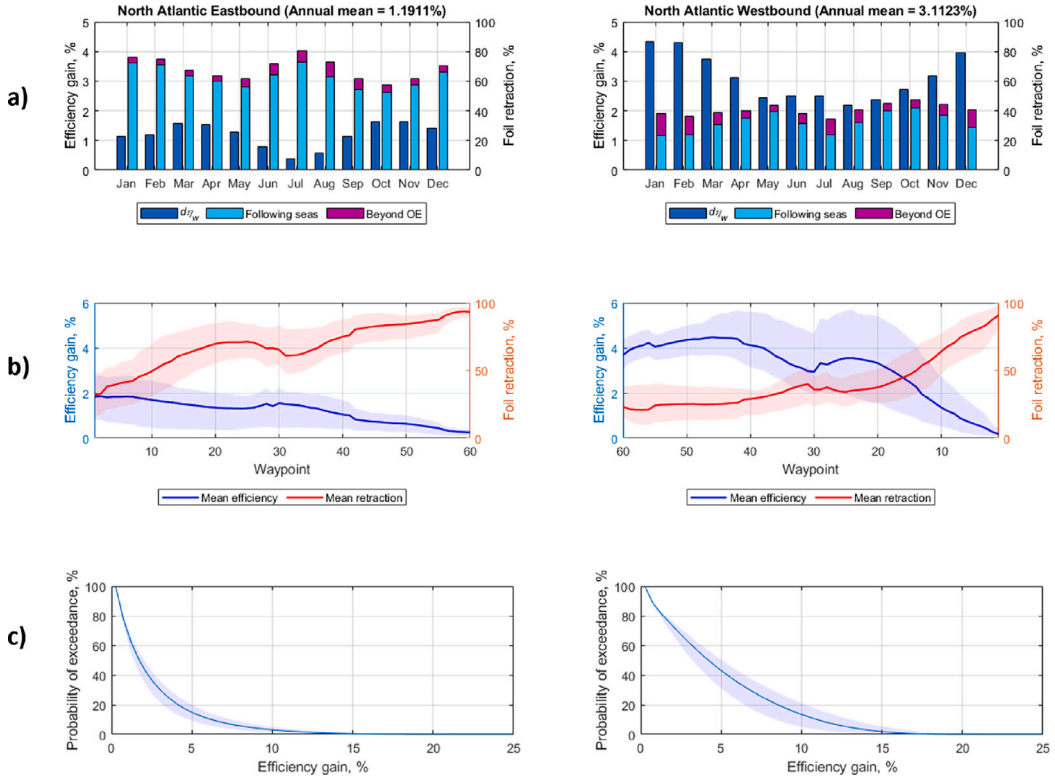

Fig. 9. Efficiency gain results for the North Atlantic route; (a) Monthly (b) Enroute (the shaded region represents the seasonal variation) and (c) Probability of exceeding an efficiency gain when the foil is deployed (the shaded region represents experimental uncertainty).

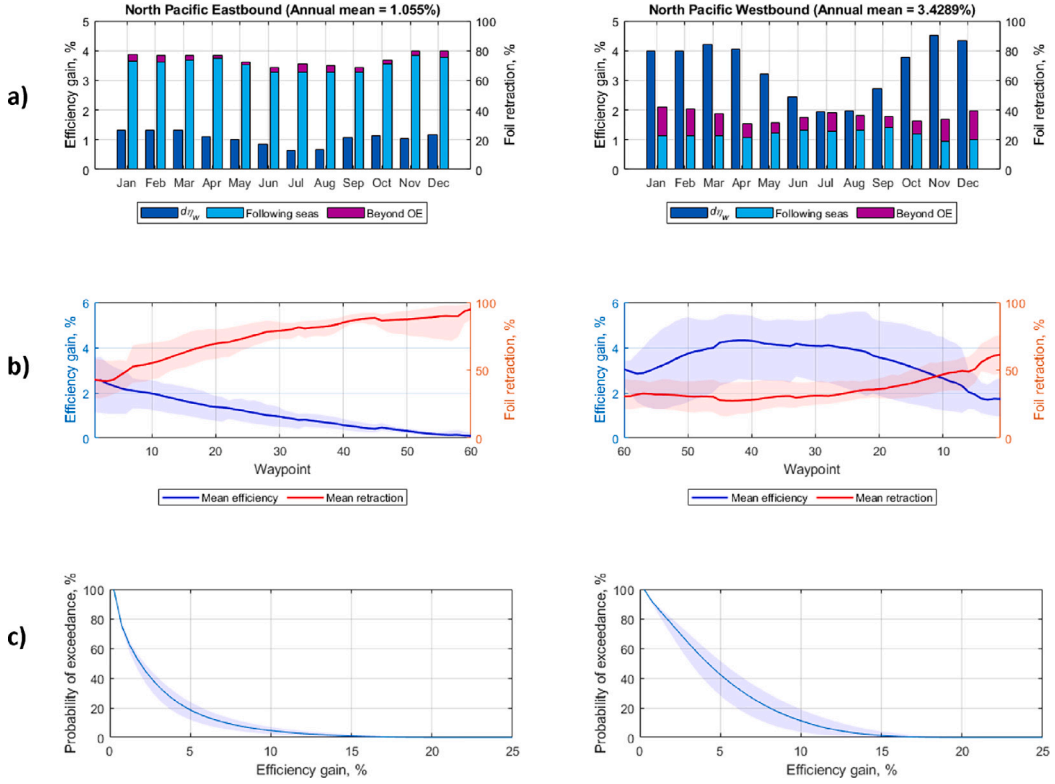

Fig. 10. Efficiency gain results for the North Pacific route; (a) Monthly (b) Enroute (the shaded region represents the seasonal variation) and (c) Probability of exceeding an efficiency gain when the foil is deployed (the shaded region represents experimental uncertainty).

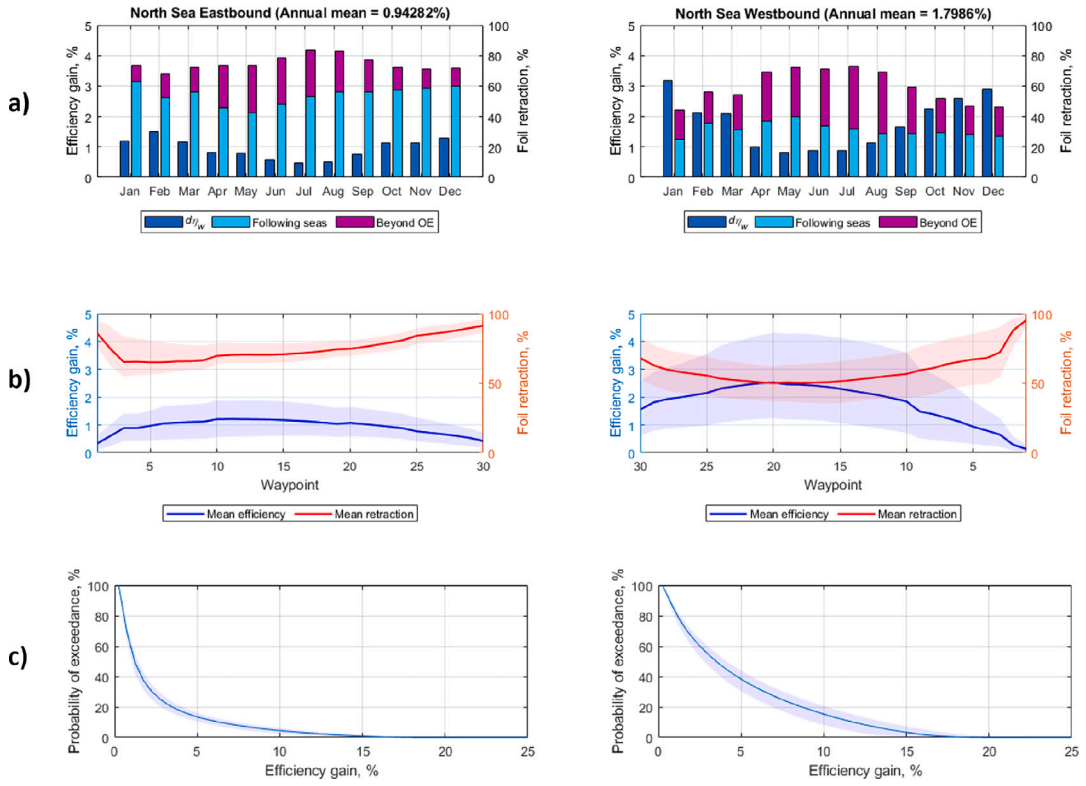

Fig. 11. Efficiency gain results for the North Sea route; (a) Monthly (b) Enroute (the shaded region represents the seasonal variation) and (c) Probability of exceeding an efficiency gain when the foil is deployed.

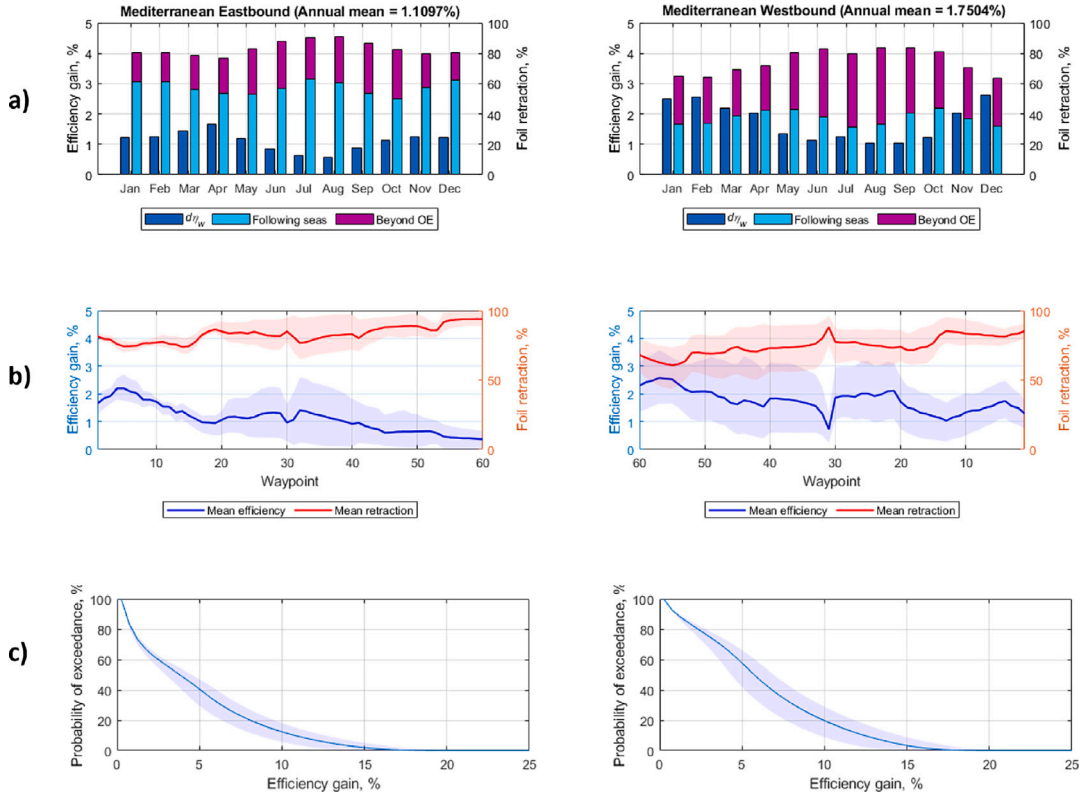

Fig. 12. Efficiency gain results for the Mediterranean route; (a) Monthly (b) Enroute (the shaded region represents the seasonal variation) and (c) Probability of exceeding an efficiency gain when the foil is deployed (the shaded region represents experimental uncertainty).

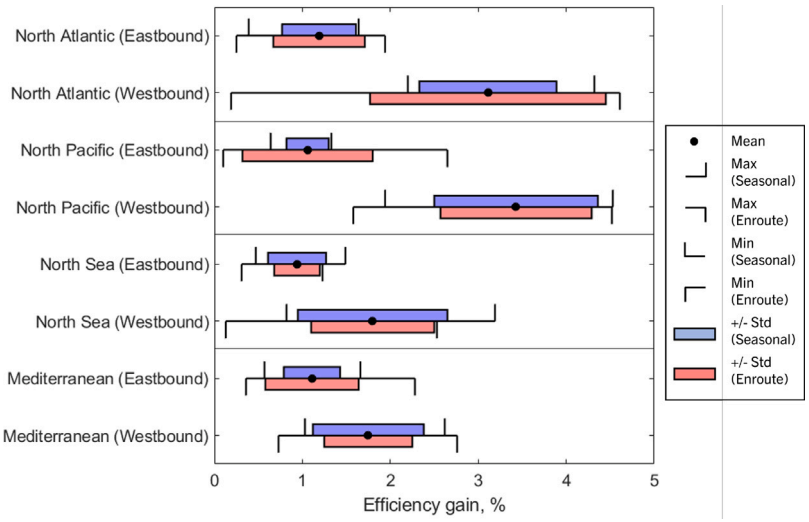

Fig. 13. Statistical analysis of the bow foil efficiency gain for seasonal variation (based on the monthly data presented in Figs. 9, 10, 11 and 12 (a)) and for enroute variation (based on the solid line presented in Figs. 9, 10, 11 and 12 (b)).

other than the effect of length scale. The methodology does, however, provide a framework for the evaluation of prospective bow foil designs, which could be expanded to perform parametric assessments by utilising a basis dataset derived from numerical simulations.

Furthermore, the results are based on a passively spring loaded bow foil system, which was designed to limit the relative angle of attack to less than the dynamic stall angle of the foil. The bow foil could be optimised using active control to maximise the resultant thrust, which has been proposed to improve efficiency. The pitching mechanism of the foil presents an interesting design consideration. Previous research has investigated the use of fixed foils (Bockmann et al., 2018; Feng et al., 2014; Huang et al., 2016), passively spring loaded foils (Bockmann and Steen, 2014; Bowker and Townsend, 2022) and actively pitched foils (Belibassakis and Politis, 2013; Belibassakis and Filippas, 2015; Bockmann and Steen, 2014; Huang et al., 2016; Belibassakis et al., 2022). In comparison to previous studies (Feng et al., 2014; Bockmann et al., 2018), the foil size implemented for this assessment is relatively large, which is considered beneficial for maximising efficiency but costly for structural design and the feasibility of retraction. The results provided in this article are therefore an indicative example of how the method is implemented and does not represent that of a real design.

The aforementioned limitations refer to the basis dataset and not the overall methodology, which is subject to several assumptions. The foil deployment is defined by an operational envelope, which includes the following assumptions; maximum wave steepness of 1/20, minimum significant wave height of 1 m and zero bow foil effectiveness in following seas. These limits require further work to verify the assumptions and the results will vary depending on the values set. The methodology also contains several assumptions regarding the extrapolation of the experimental dataset, which include the cos-squared relationship, the linear spectral response and the response in short-crested waves. These assumptions could be tested and improved using model scale tests in irregular, short-crested and oblique waves. Except for the probability of exceedance analysis, the current method assumes that the probability of wave heading is representative of the entire dataset for a particular location and is, therefore, independent of individual sea states. Further work could increase the complexity by introducing joint probabilities of sea state and wave direction ($POCC_{H_s,T,\chi} = POCC_{H_s,T} \cap POCC_{\chi}$). An additional assumption is that the foil retraction process is instantaneous, which is unlikely to be the case in reality and could involve some speed loss or additional drag during the process. For future bow foil designs, that have a detailed understanding of the retraction method, a coefficient could be included in the current analysis to account for such losses.

4.5. Practical considerations

The current methodology provides a useful guide on bow foil performance with respect to ship length and the incident wave environment. For future bow foil designs, this method could be expanded to consider structural loading (i.e. cyclic fatigue), economic analysis and a range of speeds.

The economic and structural considerations could be combined to assess the compromise between maximising efficiency and retaining structural integrity within the context of cost and profitability. This could be achieved by expanding the current method to assess the cyclic forces acting on the foil, in conjunction with a life-cycle cost analysis tool, such as Bui et al. (2022). Although the process of foil retraction has been resolved for small ships (Wavefoil, 2019), the engineering challenges associated with larger systems require consideration in order to realise the potential of deploying bow foils on larger ships such as bulk carriers.

Further considerations include the ship speed, which in this case is specific to the speed tested at model scale. Since the results follow Froude scaling laws, each ship length corresponds to a full scale equivalent ship speed, shown in Table 3. The results cannot consider a change in ship speed which would shift the bow foil optimal wavelength to ship length ratio and, therefore, the operational envelope. This is due to a change in wave encountered frequency which is proportional to ship speed. An expansion of the dataset for different ship speeds would yield new transfer functions for the change in delivered power, creating a parallel dataset that could be used to assess the effect of ship speed.

5. Conclusions

This paper presents a probabilistic methodology to predict bow foil performance. A key outcome from the method is the ability to assess bow foil performance worldwide for varying ship sizes and routes. The ship length is shown to dominate the effectiveness of the bow foil for different regions worldwide, which is principally associated with matching the length of the ship to the most prevalent local encountered wavelength. The results suggest that the most suitable conditions for effective bow foil operation is in waves with an average encountered wavelength similar to that of the ship length and a direction that opposes the ship's heading.

The results also show that the percentage foil retraction is a significant factor in operating bow foils, due to seasonal and enroute variation, and the relative wave direction. Given the adverse impact of

foil retraction on the overall efficiency gains, it is recommended that further research is focused on increasing the operational envelope of bow foils to maximise effective utilisation at sea.

Bow foils have the scope for improvement through design optimisation, particularly towards enlarging the operational envelope. Since this method can also be applied to a numerical dataset (i.e. from simulations), it could be used to optimise future bow foil designs for specific ships and routes.

CRediT authorship contribution statement

J.A. Bowker: Conceptualization, Methodology, Validation, Formal analysis, Investigation, Data curation, Writing – original draft, Visualization. **N.C. Townsend:** Methodology, Investigation, Writing – review & editing, Supervision, Funding acquisition.

Declaration of competing interest

The authors declare the following financial interests/personal relationships which may be considered as potential competing interests: James Bowker reports financial support was provided by Horizon 2020.

Data availability

Data will be made available on request.

Acknowledgements

This research was supported by the EU as part of the SeaTech project (https://seatech2020.eu/).

This project has received funding from the European Union's Horizon 2020 research and innovation programme under grant agreement No 857840.

The opinions expressed in this document reflect only the author's view and in no way reflect the European Commission's opinions. The European Commission is not responsible for any use that may be made of the information it contains.

References

Abkowitz, M.A., 1959. The effect of antipitching fins on ship motions. In: The Society of Naval Architects and Marine Engineers, SNAME'74, Trinity Place, New York, USA, Volume 67, 1959, Paper No. 1, SNAME Transactions 1959.

Belibassakis, K., Bleuanus, S., Vermeiden, J., Townsend, N., 2021. Combined performance of innovative biomimetic ship propulsion system in waves with dual fuel ship engine and application to short-sea shipping. In: The 31st International Ocean and Polar Engineering Conference.

Belibassakis, K.A., Filippas, E.S., 2015. Ship propulsion in waves by actively controlled flapping foils. Appl. Ocean Res. 52, 1–11. http://dx.doi.org/10.1016/j.apor.2015.04.009, URL https://www.sciencedirect.com/science/article/pii/S0141118715000541.

Belibassakis, K., Filippas, E., Papadakis, G., 2022. Numerical and experimental investigation of the performance of dynamic wing for augmenting ship propulsion in head and quartering seas. J. Mar. Sci. Eng. 10 (1), 1–24.

Belibassakis, K.A., Politis, G.K., 2013. Hydrodynamic performance of flapping wings for augmenting ship propulsion in waves. Ocean Eng. 72, 227–240. http://dx.doi.org/10.1016/j.oceaneng.2013.06.028, URL https://www.sciencedirect.com/science/article/pii/S0029801813002746.

Bockmann, E., Steen, S., 2014. Experiments with actively pitch-controlled and spring-loaded oscillating foils. Appl. Ocean Res. 48, 227–235. http://dx.doi.org/10.1016/j.apor.2014.09.004, URL https://www.sciencedirect.com/science/article/pii/S0141118714000923.

Bockmann, E., Steen, S., 2016. Model test and simulation of a ship with wavefoils. Appl. Ocean Res. 57, 8–18. http://dx.doi.org/10.1016/j.apor.2016.02.002, URL https://www.sciencedirect.com/science/article/pii/S0141118716300244.

Bockmann, E., Yrke, A., Steen, S., 2018. Fuel savings for a general cargo ship employing retractable bow foils. Appl. Ocean Res. 76, 1–10. http://dx.doi.org/10.1016/j.apor.2018.03.015, URL https://www.sciencedirect.com/science/article/pii/S0141118717304091.

Bowker, J.A., Tan, M., Townsend, N.C., 2021. Forward speed prediction of a free-running wave-propelled boat. IEEE J. Ocean. Eng. 46 (2), 402–413. http://dx.doi.org/10.1109/JOE.2020.2990143.

Bowker, J.A., Townsend, N.C., 2022. Evaluation of bow foils on ship delivered power in waves using model tests. Appl. Ocean Res. 123, 103148. http://dx.doi.org/10.1016/j.apor.2022.103148, URL https://www.sciencedirect.com/science/article/pii/S0141118722000979.

Bui, K., Perera, L., Emblemsvag, J., Schoyen, H., 2022. Life-cycle cost analysis on a marine engine innovation for retrofit: A comparative study. In: ASME 41st International Conference on Ocean, Offshore and Arctic Engineering. OMAE, Hamburg, Germany.

Cummins, W., Bales, S., 1980. Extreme value and rare occurrence statistics for Nothern Hemisphere shipping lanes. In: 5th STAR. Coronado, California.

De Silva, L.W.A., Yamaguchi, H., 2012. Numerical study on active wave devouring propulsion. J. Mar. Sci. Technol. 17 (3), 261–275. http://dx.doi.org/10.1007/s00773-012-0169-y.

Dybdahl, K., 1988. Foilpropellen kan revolusjonere skipsfarten. Teknisk Ukebl./Tek. 39, 10–11.

Feng, P., Ma, N., Gu, X., 2014. A practical method for predicting the propulsive performance of energy efficient ship with wave devouring hydrofoils at actual seas. Proc. Inst. Mech. Eng. M 228 (4), 348–361. http://dx.doi.org/10.1177/1475090213489674, URL https://journals.sagepub.com/doi/abs/10.1177/1475090213489674.

Filippas, E.S., 2015. Augmenting ship propulsion in waves using flapping foils initially designed for roll stabilization. Procedia Comput. Sci. 66, 103–111. http://dx.doi.org/10.1016/j.procs.2015.11.013, URL https://www.sciencedirect.com/science/article/pii/S1877050915033621.

Filippas, E.S., Papadakis, G.P., Belibassakis, K.A., 2020. Free-surface effects on the performance of flapping-foil thruster for augmenting ship propulsion in waves. J. Mar. Sci. Eng. 8 (5), 357, URL https://www.mdpi.com/2077-1312/8/5/357.

Huang, S., Wu, T., Hsu, Y., Guo, J., Tsai, J., Chiu, F., 2016. Effective energy-saving device of Eco-Ship by using wave propulsion. In: 2016 Techno-Ocean (Techno-Ocean). pp. 566–570. http://dx.doi.org/10.1109/Techno-Ocean.2016.7890719.

IMO, 2013. ANNEX 14. Resolution of MPEC 231(65). International Maritime Organisation (IMO).

Isshiki, H., Murakami, M., 1984. A theory of wave devouring propulsion (4th report) a comparison between theory and experiment in case of a passive-type hydrofoil propulsor. J. Soc. Nav. Archit. Japan 156, 102–114.

ITTC, 2014. Guide to the Expression of Uncertainty in Experimental Hydrodynamics. Quality Systems Group of the 27th ITTC.

ITTC, 2021a. Final Report and Recommendations to the 29th ITTC. The Special Committee on Energy Saving Methods.

ITTC, 2021b. Prediction of Power Increase in Irregular Waves from Model Tests. Seakeeping Committee of the 29th ITTC.

Jakobsen, E., 1981. The foil propeller, wave power for propulsion. In: 2nd International Symposium on Wave and Tidal Energy, 1981. pp. 363–369, URL https://ci.nii.ac.jp/naid/80001169029/en/.

Naito, S., Isshiki, H., 2005. Effect of bow wings on ship propulsion and motions. Appl. Mech. Rev. 58 (4), 253–268. http://dx.doi.org/10.1115/1.1982801.

Naito, S., Isshiki, H., Fujimoto, K., 1986. Thrust generation of a fin attached to a ship in waves. J. Kansai Soc. Nav. Archit..

Nikolaev, M.N., Savitsky, A., Senkin, Y., 1995. Basics of calculation of the effciency of a ship with propulsor of the wing type. Sudostroenie 4, 7–10.

NOAA, NCEP, 2021. WaveWatch III. https://polar.ncep.noaa.gov/waves/hindcasts/nopp-phase2.php, accessed: 30-10-2021.

Perrault, D.E., 2021. Probability of sea condition for ship strength, stability, and motion studies. J. Ship Res. 65 (1), 1–14.

Schlining, B., Signell, R., Cosby, A., 2009. Nctoolbox. Github repository, https://github.com/nctoolbox/nctoolbox.

Stefun, G.P., 1959. Model experiments with fixed bow antipitching fins. J. Ship Res. 3 (03), 14–23. http://dx.doi.org/10.5957/jsr.1959.3.3.14.

Terao, Y., Isshiki, H., 1991. Wave devouring propulsion sea trial. In: Eighteenth Symposium on Naval Hydrodynamics. 297–296.

Wavefoil, 2019. Press release. www.wavefoil.com/pressrelease, accessed: 18-08-2021.

Wu, T.N., Guo, J., Chen, Y.N., Chen, W.C., 1996. Experimental study of ship pitching motion reduction using anti-pitching fins. In: Proceedings of the JFPS International Symposium on Fluid Power, 1996. pp. 223–228. http://dx.doi.org/10.5739/isfp.1996.223, (3).

Wu, L., Xu, Y., Wang, Q., Wang, F., Xu, Z., 2017. Mapping global shipping density from AIS data. J. Navig. 70.